Imaging optical singularities: Understanding the duality of C-points and optical vortices

Enrique J. Galvez, Brett L. Rojec and Kevin R. McCullough

Department of Physics and Astronomy, Colgate University, 13 Oak Drive, Hamilton, New York 13346, U.S.A.

ABSTRACT

We image optical singularities by exploiting the connection between scalar and vector fields. We examine the sensitivity of optical vortices to perturbations and suggest a method of study via imaging polarimetry of the optical field. This is possible by converting optical vortices to polarization-singularity C-points. We present the deliberate creation of C-points using a superposition of two circularly polarized beams of opposite helicity, with a phase vortex in one and a planar wavefront in the other. We present a theoretical analysis and measurements of the transformation of C-points from lemon to star, going through the monstar stage. We do this by varying the phase gradient of the optical vortex.

Keywords: Poincare beams, Optical Vortices, Laguerre-Gauss modes, Polarization singularities

1. INTRODUCTION

Optical vortices are ubiquitous in random wave fields.[1] Their dark core implies a circulating phase in the field surrounding them. Several classes of paraxial beams can propagate carrying optical vortices. They are characterized by the topological charge ℓ of the vortex, which represents the number of times that the phase advances by 2π per turn around the vortex. In Laguerre-Gauss (LG) eigenmodes, optical vortices are structures located at the center of the mode. Beams in superpositions of LG eigenmodes can carry arrays of optical vortices that move or rotate transversely as the light propagates. The latter motion is caused by the distinct Gouy phases of the component eigenmodes.[2] Theoretically, optical vortices are identified by zeros in both the real and imaginary components of the field.[1] Experimentally, optical vortices are unambiguously identified by the surrounding field: via dislocations (forks) in the interference pattern formed by non-collinear interference with a reference field.[3,4] or by phase-shifting interferometry.[5]

Polarization singularities are the vector-field counterparts of scalar singularities. The most important singularities of this kind are the C-points.[6] These are points of circular polarization that are surrounded by a field of points with elliptical polarization. The semi-major axis of the ellipses rotates about the C-point. Two of the three fundamental types of C-points are the lemon and the star. They occur when the semi-major axis of the ellipses rotates around the C-point in a counter-clockwise or clockwise fashion, respectively, as we follow them around the C-point. As shown in detail in this article, a C-point singularity, in its simplest form, is the superposition of a circularly-polarized optical vortex field with an oppositely-polarized planar field.[7,8]

Optical vortices are very sensitive to perturbations, to the point that optical vortices with topological charge greater than one are difficult to preserve and measure.[2,9] The latter is often due to the perturbating action of the imaging field or inhomogeneities in the medium through which the light is traveling. In this article we investigate the imaging aspect of vortices further, by converting the optical vortex into a polarization-singularity C-point, and then diagnosing the light field using imaging polarimetry. The advantage of this method is that it does not perturb the vortex field at all because it uses a reference field that is polarized orthogonally to the vortex field.

The study of polarization singularities on demand has been possible with (full) Poincaré modes, produced via superpositions of orthogonal polarization eigenstates in distinct spatial modes.[10–13] However, until now spatial

Further author information: (Send correspondence to E.J.G.)
E.J.G.: E-mail: egalvez@colgate.edu, Telephone: 1 315 228 7205
Proceedings of SPIE **8637**, 863706 (2013).

eigenmodes have been used to produce only stars and lemons. In this work we make C-point monstars by preparing superpositions of states that contain optical vortices with uneven phase gradients.

This article is organized as follows: Section 2 has a theoretical description of the problem, which includes a description of the scalar and vortex fields; Section 3 describes the apparatus; and Section 4 presents the two types of results of this work.

2. THEORETICAL CONSIDERATIONS

We will begin by presenting the theoretical basis of the experiments. The work involves scalar and vector singularities, so we devote separate subsections to them. We have also developed a theoretical treatment of monstars, which is presented in the third subsection.

2.1. Scalar Singularities: Optical Vortices

LG modes are denoted by two indices: the radial index p and the angular index ℓ. The latter is also the topological charge of the vortex contained in the mode. The scalar component of the field in a $p = 0$, singly-ringed or "doughnut" LG mode is given by

$$LG_0^\ell = A_\ell r^{|\ell|} \mathrm{e}^{\mathrm{i}\ell\phi} GW. \tag{1}$$

The optical vortex of topological charge ℓ, located at the origin of the beam's transverse plane, is specified by the factor $r^{|\ell|}\mathrm{e}^{\mathrm{i}\ell\phi}$. LG beams also carry a Gaussian envelope, given by

$$G = \mathrm{e}^{-r^2/w^2}, \tag{2}$$

with w being the beam's half width. Other terms in Eq. 1 are the normalization constant

$$A_\ell = \left(\frac{2^{|\ell|+1}}{\pi|\ell|!)}\right)^{1/2} \frac{1}{w^{|\ell|+1}}; \tag{3}$$

and the phase term

$$W = \mathrm{e}^{\mathrm{i}(x^2+y^2)/(2R)-\varphi}, \tag{4}$$

where R is the radius of curvature of the wavefront and φ is the Gouy phase. In this work we will ignore the phase term as we will not examine propagation effects. The radius of the ring (i.e., where intensity is maximum) is

$$r_\ell = \sqrt{\frac{\ell}{2}} w. \tag{5}$$

Previous studies by our group showed that when an LG beam with topological charge $|\ell| > 1$ and intensity I_ℓ is superimposed with a collinear $\ell = 0$ charged vortex of intensity I_0, results in the breakup of the multiply-charged vortex into $|\ell|$ singly charged vortices.[2] The latter are arranged in a angularly symmetric pattern, and equidistant from the beam center by

$$r_\mathrm{v} = \frac{w}{\sqrt{2}} \left(|\ell|! \frac{I_\ell}{I_0}\right)^{1/2|\ell|}. \tag{6}$$

Figure 1 shows an example of the case when $\ell = 3$. The image of the $\ell = 3$ mode alone is shown in frame (a), and the superposition of equal intensity modes with $\ell = 3$ and $\ell = 0$ is shown in frame (b). The spiral arms of the measured mode are due to the wavefront curvature of the two beams. Frames (c) and (d) show a computation of the phase map for the cases of frames (a) and (b), respectively, but not accounting for the wavefront curvature. The sequence of frames shows how the LG mode with $\ell = 3$ is split into three $\ell = 1$ vortices by the addition of a Gaussian mode with intensity I_0.

The situation for other values of ℓ is similar. What is notable is the sensitivity of the vortices in to an additional $\ell = 0$ field. A measure of this sensitivity is the graph of r_v from Eq. 6, shown in Fig. 2. We see that r_v rises quite quickly as a function of the intensity of an $\ell = 0$ field. The rise increases rapidly with ℓ. For

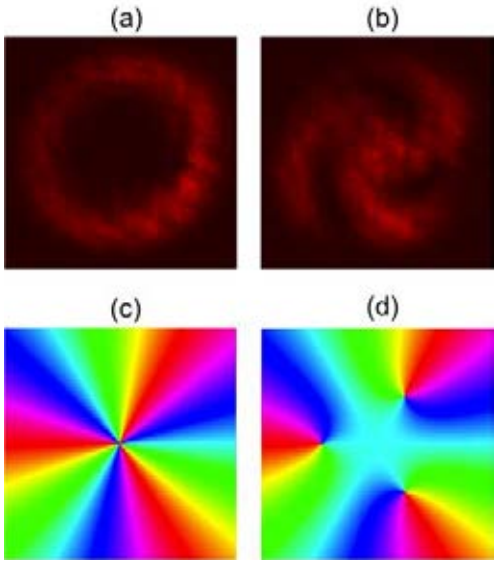

Figure 1. Frames (a) and (b) show images of the LG mode $\ell = 3$: Frame (a) shows the LG mode alone; frame (b) shows the $\ell = 3$ mode superimposed with an $\ell = 0$ mode of equal intensity. Frames (c) and (d) correspond to the calculated color-coded phase maps for cases (a) and (b), respectively.

example, for the case of combining $\ell = 6$ with $\ell = 0$, the broken-up vortices reach a beam-width away from the center of the beam with barely under a tenth of the $\ell = 0$ intensity. That is, the greater the number of vortices that share a physical location, the higher is their propensity to be split by the presence of a perturbing Gaussian field. This rise is even greater if the perturbing field has a flatter amplitude vs. r (e.g., with higher half-width w). We can understand this the following way: the higher the value of ℓ, the higher the radius of the mode r_ℓ. Since the split vortices form at locations where the intensity of the perturbing field equals that of the multiply charged mode (i.e., $r_{\rm v}$),[2] the radial distance of these locations increases with ℓ faster if the perturbing mode has a greater width.

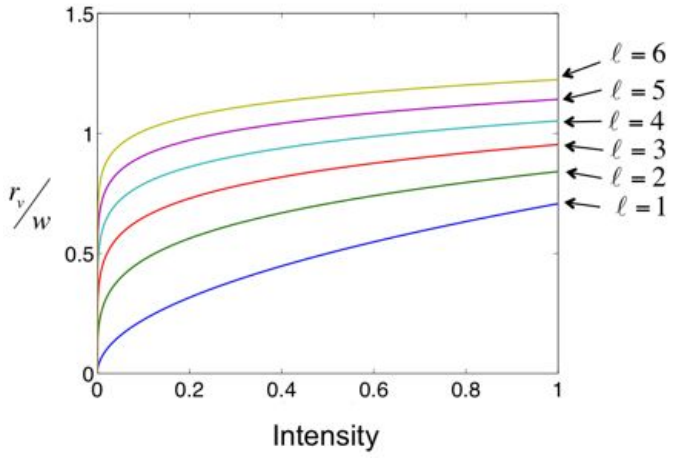

Figure 2. Graph of the radial position of vortices in an LG beam with a topological charge ℓ as a function of the relative intensity of a perturbing field with $\ell = 0$.

2.2. Vector Singularities: C-points

The simplest form of polarization singularity is a point in the elliptical vector field where the orientation of the semimajor axis of the ellipse is undefined: a circle. This is the C-point. The state of polarization can be represented conveniently using the Poincaré sphere, shown in Fig. 3, where each point on the surface of the sphere defines a unique state of polarization, with points of equal latitude having equal ellipticity, and points of equal longitude having equal orientation of their semimajor axes (i.e. angle formed with the x-axis). Northern and southern hemispheres of the sphere correspond to different handedness, and with the poles representing the states of circular polarization. We can represent the state of polarization via their polar coordinates on the sphere:[11,12]

$$\psi = e^{\mathrm{i}\theta}\cos\chi\hat{e}_R + e^{-\mathrm{i}\theta}\sin\chi\hat{e}_L, \tag{7}$$

where $\hat{e}_R$ and $\hat{e}_L$ represent the states of circular polarization, right (RCP) and left (LCP), respectively. In this representation χ and θ specify the shape and orientation of the ellipse, respectively. The ellipticity of the state is related to the ratio of the amplitudes of the polarization components via

$$\epsilon = \frac{b}{a} = \tan(\pi/4 - \chi), \tag{8}$$

where a and b are the semimajor and semiminor axes of the ellipse, respectively. The orientation of the ellipse, or the angle that the semimajor axis of the ellipse forms with the x-axis, θ, is half the phase difference between the two components.

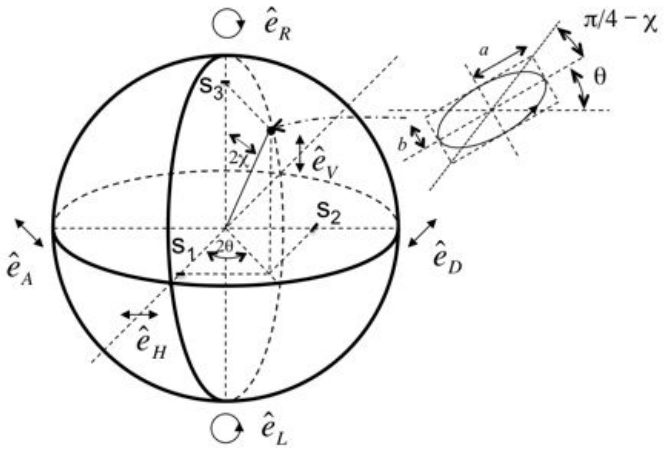

Figure 3. Poincare sphere representing all states of polarization.

The coordinates of the points on the surface of the sphere, or Stokes parameters S_1, S_2 and S_3, can be used to identify the C-point. If we define[14–16]

$$\sigma = S_1 + \mathrm{i}S_2, \tag{9}$$

then the orientation of the semimajor axis of the ellipse is given by

$$\theta = \arg(\sigma)/2. \tag{10}$$

We can represent a C-point by the superposition of a planar field and an optical vortex.[17] The handedness of the C-point is the handedness of the polarization of the field with the planar wavefront. For example, the field of a left-handed C-point can be represented by

$$\psi = re^{\mathrm{i}\ell\phi}\hat{e}_R + a\hat{e}_L, \tag{11}$$

where a is a constant and $|\ell| = 1$. The ellipticity of the ellipse at a given point is determined by a/r, and its orientation by ϕ. When $\ell = +1$ the C-point is a lemon, whereas when $\ell = -1$ it is a star.[8] This is shown in

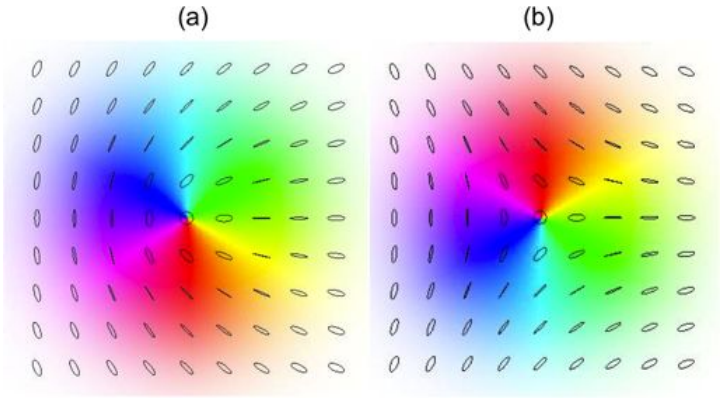

Figure 4. C-points are generated by a right-circularly polarized LG beam carrying and optical vortex with $\ell = +1$ (a) and $\ell = -1$ (b), and superimposed collinearly with an oppositely polarized LG beam with $\ell = 0$. These are the lemon and star types of C-points, respectively. False color reveals the orientation of the semimajor axis of the ellipses, and the color saturation is proportional to the intensity of the beam.

Figs. 4(a) and 4(b), respectively. Because the two fields are orthogonal, the position of the C-point is the same as the position of the optical vortex. The C-point index, specifying the rotation of the axes of the ellipse per turn around the C-point, is $I_C = +1/2$ for the lemon and $I_C = -1/2$ for the star.[8,17] Furthermore, in the converse direction, we can use the type of C-point to obtain the sign of the topological charge of the underlying optical vortex.

Polarization fields provide an optics analogy to the topology of Gaussian surfaces.[18] C-points are equivalent to umbilical points of the surface, where the principal planes of curvature are undefined.

2.3. Finding Monstardom

Monstars are singularities that capture the handedness of lemons and the topology of stars. They are ubiquitous,[19] but have a more complex construction than lemons and stars. Several prescriptions have been proposed for making monstars.[7,8,20] Here we present a simpler approach that adapts well to the experiments. To make a C-point monstar we modify Eq. 11 to the form

$$\psi = (\cos\beta\, re^{i\ell\phi} + \sin\beta\, re^{-i\ell\phi}e^{i\gamma})\hat{e}_R + a\hat{e}_L, \tag{12}$$

where β controls the superposition of two singly-charged vortices of opposite handedness, and γ is the phase in between them. This way, for $\beta = 0$ and $\beta = \pi/2$ the vortex is purely $\ell = +1$ and $\ell = -1$, respectively, both of which contain a constant angular phase gradient. For $\beta = \pi/4$ there is no vortex; the composite right-circularly polarized mode is a first-order Hermite-Gauss mode. For all other values of β the composite mode has a central vortex of topological charge equal to that of the mode with the largest amplitude. However, for this case, the angular phase gradient of the composite is not constant. In addition, the relative phase γ rotates the composite mode by $\gamma/2$.

Without loss of generality we can assume that the phase of the left circularly polarized plane wave of Eq. 12 is zero. The phase of the right circularly polarized state is given by

$$\alpha = \tan^{-1}\left[\frac{\tan\phi + \tan\beta(\sin\gamma - \cos\gamma\tan\phi)}{1 + \tan\beta(\cos\gamma + \sin\gamma\tan\phi)}\right]. \tag{13}$$

The orientation of the ellipses in the state of polarization is given by

$$\theta = \frac{\alpha}{2}. \tag{14}$$

C-points are characterized by two properties: the C-point index, $+1/2$ for lemon and monstar, and $-1/2$ for star; and the number of angles in which the orientation of the ellipses is equal to the angular orientation, which is three for star and monstar, and one for lemon.[8, 18] We will map the C-points via Eq. 12 and the second characteristic. This condition is represented by

$$\theta = \phi. \tag{15}$$

Combining Eqs. 13, 14 and 15 we get a cubic equation in $x = \tan\phi$:

$$ax^3 + bx^2 + cx + d = 0, \tag{16}$$

where

$$\begin{aligned} a &= \tan\beta\cos\gamma - 1 && (17)\\ b &= -3\tan\beta\sin\gamma && (18)\\ c &= -1 - 3\tan\beta\cos\gamma && (19)\\ d &= \tan\beta\sin\gamma && (20) \end{aligned}$$

As is well known, Eq. 16 has a discriminant given by

$$\Delta = 18abcd - 4b^3d + b^2c^2 - 4ac^3 - 27a^2d^2. \tag{21}$$

If $\Delta \geq 0$ there are three real roots to the equation (star, monstar), and when it is $\Delta < 0$ it has one real root (lemon). Thus, β and γ map the regions of possible C-points in a two-dimensional space. This fact has been shown previously by Dennis.[20] However, here we use different variables.

As an example, we present the case where the C-points are least skewed, which occurs when $\gamma = \pi$. For this case, the phase difference between the two polarization eigenstates in the region surrounding the C-point is

$$\alpha = \tan^{-1}(C\tan\phi), \tag{22}$$

where

$$C = \frac{1+\tan\beta}{1-\tan\beta}. \tag{23}$$

Solving Eq. 15 for this case gives as solutions

$$\phi = 0 \tag{24}$$

and

$$\phi = \pm\tan^{-1}\sqrt{1-\frac{2}{C}}. \tag{25}$$

The latter solutions are real when $C \geq 2$, or when $\beta \geq \beta_0$, with $\beta_0 = \tan^{-1}(1/3)$. Thus, the solutions of Eq. 13 with the conditions 15 and $\gamma = \pi$ give three regimes:

- Lemon: $0 \leq \beta < \beta_0$
- Monstar: $\beta_0 \leq \beta < \pi/4$
- Star: $\pi/4 < \beta \leq \pi/2$.

Figure 5 shows the full map of the possible values of β and γ. It has three regions where lemons, monstars and stars are possible. We also show the computed polarization maps for various cases where $\gamma = \pi$. This map is qualitatively similar to that of Dennis.[20] For points with $\gamma \neq \pi$ the angles that satisfy the condition of Eq. 15 do not form a symmetric arrangement. Table 1 gives a few examples. Figure 5 also shows one such pattern for $\beta = 43^\circ$ and $\gamma = 120^\circ$.

Table 1. Examples of angles defining monstars.

β	γ	$\theta = \phi$
45°	0.1°	0.03°, −89.95°, −89.98°
44°	45°	11.15°, −71.2°, −74.9°,
43°	90°	22.1°, −47.4°, −64.7°
43°	120°	29.4°, −31.3°, −58.1°
18.43°	180°	0°, 0°, 0°
20°	180°	0°, ± 14.55
30°	180°	0°, ±34.26°
40°	180°	0°, ±42.25°

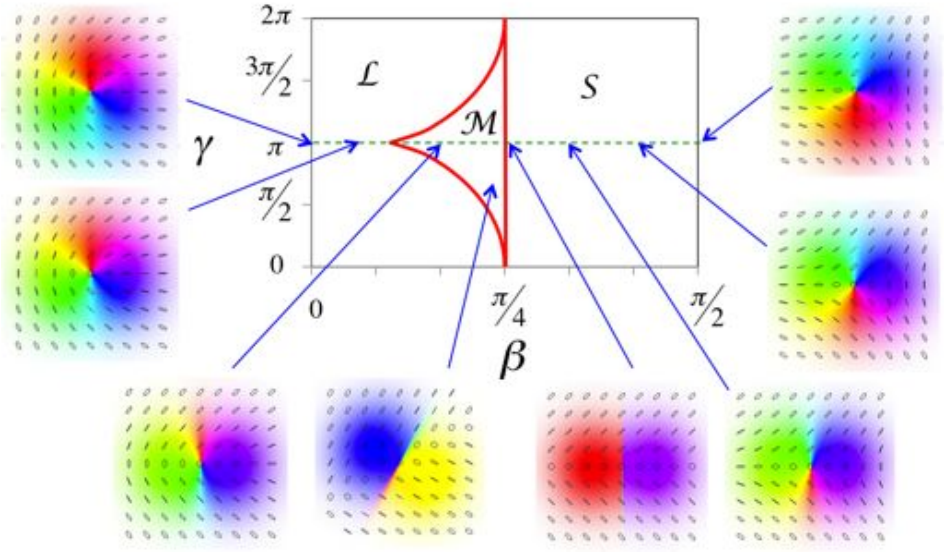

Figure 5. Map of possible configurations of C-points: lemons ($\mathcal{L}$), monstars ($\mathcal{M}$) and stars ($\mathcal{S}$). Inserts show examples of computed polarization maps.

3. APPARATUS

The apparatus used in this study is shown in Fig. 6. Linearly polarized light from a HeNe laser is expanded and spatial-filtered by a ×3 beam expander. It is then incident on a Mach Zehnder interferometer. A non-polarizing beam splitter in the input port splits the light into two beams that are incident onto a spatial light modulator (SLM) (Holoeye LC-R-2500).

The SLM is programmed with phase gratings to encode two spatial modes, as shown in the figure. The phase gratings were blazed to produce a diffracted beam at an angle of 0.5 degrees from the mirror reflection. The forked patterns of the vortex-bearing LG modes were modulated with the amplitude of the mode. The width of the amplitude-modulated mode was matched to the width of the incoming beam. The pattern for the $\ell = 0$ mode was not amplitude modulated since the input beam was already in the $\ell = 0$ mode.

The diffracted beams passed through a linear polarizer. The polarization of one of the diffracted modes was rotated by 90 degrees with a half-wave plate. One beam was sent to a mirror, while the other one was sent to a polarizing beam splitter. This way, the two modes leaving the interferometer were orthogonally polarized and collinear. A quarter-wave plate after the interferometer converted the orthogonal linear polarizations to the circular basis.[21]

Past the preparation stage, the light was sent to a set of waveplates and polarizers for polarimetry analysis.[11] Six images were recorded with a digital camera, after passage of the beam through polarization filters: linear

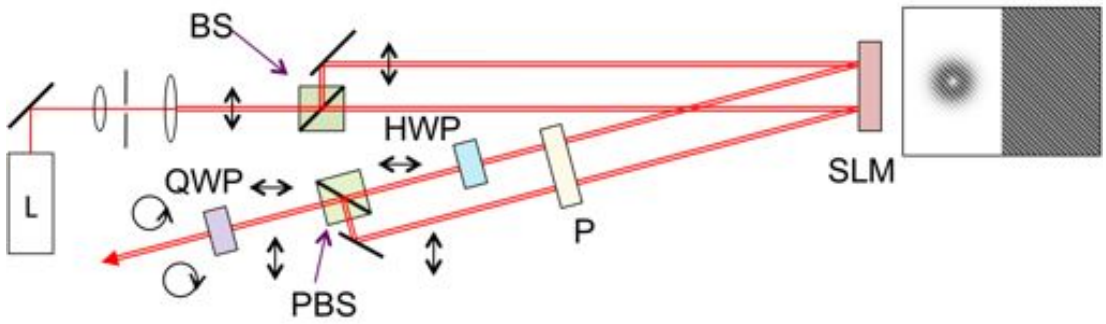

Figure 6. Apparatus used to create C-points. The main components are the spatial light modulator (SLM), polarizer (P) half-wave plate (HWP), quarter-wave plate (QWP), non-polarizing beam splitter (BS) and polarizing beam splitter (PBS). An example of the pattern encoded in the SLM is shown in the insert, with decreased fringe density for illustration purposes.

vertical, horizontal, diagonal, antidiagonal; and circular right and left. With this information we could determine the Stokes parameters,[22] and consequently the state of polarization, for each image pixel.

In our experiments, care was put in the alignment of the beams that were put into a collinear superposition. The limitations depend on our methods (interferometric, in our case) to adjust the degree of collinearity.

4. IMAGING C-POINTS AND OPTICAL VORTICES

Our experimental studies concentrated on two problems. One involved the deliberate production of polarization patterns that contained monstars, according to our analysis presented in Sec. 2.3. The second set of investigations involved the problem of finding optical vortices via polarimetry. We present two examples of this work, which is still ongoing.

4.1. Finding Monstar C-points

In a previous report by our group we showed that the two forms of C-points, lemon and star, can be formed by collinear superpositions of $\ell = 1$ and $\ell = 0$ LG modes in opposite states of circular polarization.[11] Polarimetric measurements of these two cases can be seen in Fig. 7 (a) and (c). As with the theoretical maps, the color of the figures encodes θ, the orientation of the ellipses, and the saturation of the color encodes the intensity.

We used the prescription of Sec. 2.3 to generate the two phase patterns that program the SLM. We have taken data at various angles β and γ. Figure 7(b) shows the case for $\beta = \pi/3$ and $\gamma = \pi$. There is a clear distinction between this case and that of Figs. 7 (a) and (c). In the vicinity of the C-point one can identify the

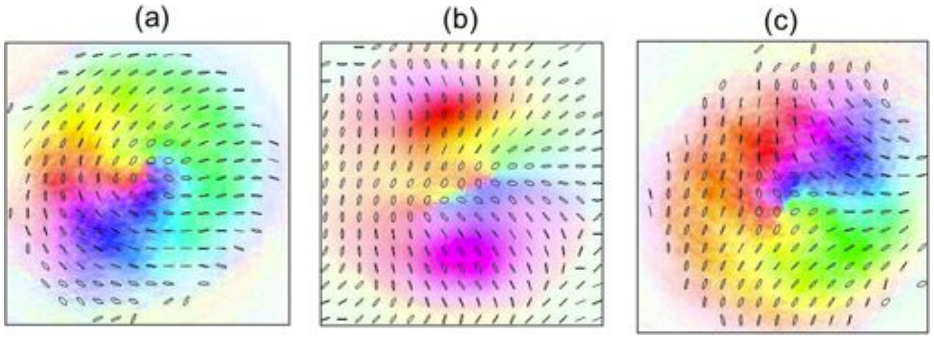

Figure 7. Measured polarization fields of prepared beams showing the three types of C-points: lemon (a), monstar (b) and star (c).

three angles at which the orientation of the ellipses matches the radial direction. That and the C-point index of $+1/2$ are the signatures of the monstar C-point. The curvature of the wavefront of the beams conspired to show that the orientation of the ellipses twists at points that are a waist away from the C-point. There are no published reports of this type of measurement of monstars, but we are aware of other groups working on the problem. Our measurements are consistent with the predictions of Eq. 12.

4.2. Imaging Optical Vortices

As mentioned earlier, the C-points of Fig. 7 were produced by the collinear superposition of orthogonal circularly-polarized modes: one with a topological charge ℓ, and the other with $\ell = 0$. We could view this as the superposition of an optical vortex and a (Gaussian) "plane wave." In the polarimetry analysis of the resulting pattern, the phase information of the vortex is encoded in the orientation of the ellipses in the field. The interesting aspect of this is that the field used to inquire about the phase of the vortex does not perturb the vortex. This is in contrast to phase shifting interferometry or forked interferograms, which involve a superposition of a reference beam with the same polarization as the signal beam, perturbing it as well.

The effect of the perturbation of a planar wavefront on a singly-charged vortex is to displace it, with the displacement depending on the amplitude and phase of the reference beam. For the case of a multiply-charged vortex, the perturbation splits the vortex into singly-charged vortices, as mentioned earlier. Thus, perturbing fields can significantly alter a field with embedded phase singularities.

In a second set of experiments we prepared multiply-charged LG modes and imaged them using our polarimetry analysis. This involved generating the perturbed mode via a computed phase hologram in half of the SLM. Figure 8(a) shows what was programmed onto the SLM when $\ell = 2$ with a perturbing intensity of 10% that of the LG mode. The hologram is also modulated by the computed intensity of the mode to minimize contributions from high-orders generated by diffraction. The right pane is a phase hologram with a linear shift, and so it deflects the incoming Gaussian beam by the same angle as the perturbed mode. The image of the perturbed mode is shown in Fig. 8(b). It shows two dark spots where optical vortices are potentially located. Note that the mode appears rotated. This is due to the Gouy rotation of the beam as it traveled from the SLM to the camera, 2 m away. The perturbed mode with right circular polarization was superposed collinearly with the $\ell = 0$ mode in left circular polarization. The imaging polarimetry of the composite vector mode is shown in Fig. 8(c). The optical vortices can be identified by the C-points, which are of the lemon/monstar type, with index $I_C = +1/2$.

The field of ellipses of Fig. 8 encodes the phase in the LG mode in the orientation of the semimajor axis of the ellipses, which is also represented by the colors in the figure.

5. CONCLUSIONS

In conclusion, we presented an analysis of polarization singularities created by the superposition of modes in opposite states of circular polarization. We developed a simple method to produce the full variety of symmetric

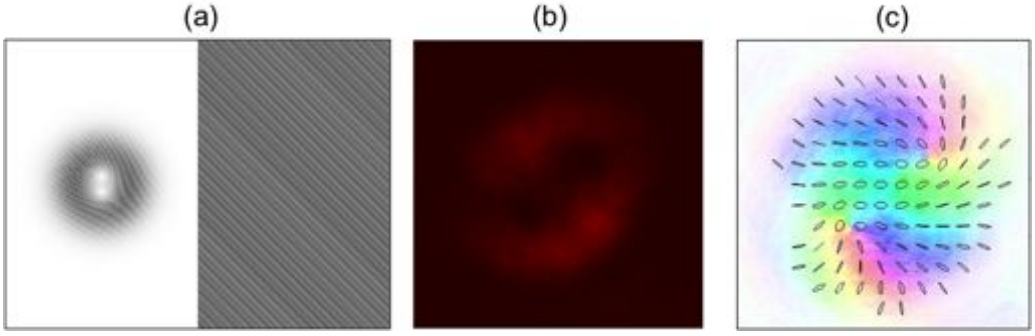

Figure 8. Determining vortex location using imaging polarimetry. The SLM was programmed with a perturbed $\ell = 2$ LG mode showing split vortices (a). The measured pattern is shown in frame (b) and the results of imaging polarimetry are shown in frame (c).

and asymmetric C-points, and in particular, monstars, which have not been produced deliberately previously. We also suggest a method to determine the location and characteristics of scalar fields and vortices using imaging polarimetry.

ACKNOWLEDGMENTS

We thank M.R. Dennis, T. Tucker and G. Milione for stimulating discussions. This work was funded by National Science Foundation grant PHY-0903972, Air Force contract FA8750-11-2-0034, and by Colgate University.

REFERENCES

1. M.V. Berry and M.R. Dennis, "Phase Singularities in Isotropic Random Waves," Proc. R. Soc. London A **456**, 2059–2079 (2000).
2. S.M. Baumann, D.M. Kalb, L.H. MacMillan, and E.J. Galvez, "Propagation dynamics of optical vortices due to Gouy phase," Opt. Express **17**, 9818–9827 (2009).
3. V.Yu. Bazhenov, M.V. Vasnetsov, and M.S. Soskin, "Laser beams with screw dislocations in their wavefronts," JETP Lett. **52**, 429-431 (1990).
4. E.J. Galvez, N. Smiley, and N. Fernandes, "Composite optical vortices formed by collinear Laguerre-Gauss beams," Proc. SPIE **6131**, 19-26 (2006).
5. J. Leach, E. Yao, and M.J. Padgett, "Observation of the vortex structure of a non-integer vortex beam," New J. Phys. **6**, 1–8 (2004).
6. J.F. Nye, *Natural Focusing and Fine Structure of Light* (IOP, 1999).
7. M.V. Berry, "Geometry of phase and polarization singularities, illustrated by edge diffraction and the tides," Proc. SPIE **4403**, 1-12 (2001).
8. M.R. Dennis, "Polarization singularities in paraxial vector fields: morphology and statistics," Opt. Commun. **213**, 201–221 (2002).
9. F. Ricci, W. Loffler, and M.P. van Exter, "Instability of higher-order optical vortices analyzed with a multi-pinhole interferometer," Opt. Express **20**, 22961–22975 (2012).
10. A.M. Beckley, T.G. Brown, and M.A. Alonso, "Full Poincaré beams," Opt. Express **18**, 10777–10785 (2010).
11. E.J. Galvez, S. Khadka, W.H. Schubert, and S. Nomoto, "Poincaré-beam patterns produced by nonseparable superpositions of LaguerreGauss and polarization modes of light," Appl. Opt. **51**, 2925-2934 (2012).
12. E.J. Galvez and S. Khadka, "Poincaré modes of light," Proc. SPIE **8274**, 82740Y 1-8 (2012).
13. F. Cardano, E. Karimi, S. Slussarenko, L. Marrucci, C. de Lisio, and E. Santamato, "Polarization pattern of vector vortex beams generated by q-plates with different topological charges," Appl. Opt. **51**, C1-C6 (2012).
14. I. Freund, "Poincaré vortices," Opt. Lett. **26**, 1996–1998 (2001).
15. I. Freund, A.I. Mokhum, M.S. Soskin, O.V. Angelsky, and I.I. Mokhum "Stokes singularity relations," Opt. Lett. **27**, 545–547 (2002).
16. M.S. Soskin, V. Denisenko, and I. Freund, "Optical polarization singularities and elliptic stationary points," Opt. Lett. **28**, 1473–1477 (2003).
17. I. Freund "Polarization singularity indices in Gaussian laser beams," Opt. Commun. **201**, 251–270 (2002).
18. M.V. Berry and J.H. Hannay, "Umbilic points on Gaussian random surfaces," J. Phys. A **10**, 1809–1821 (1977).
19. I.O. Buinyi, V.G. Denisenko, and M.S. Soskin, "Topological structure in polarization resolved conoscopic patterns for nematic liquid crystal cells," Opt. Commun. **282**, 143–155 (2010).
20. M.R. Dennis, "Polarization singularity anisotropy: determining monstardom," Opt. Lett. **33**, 2572–2574 (2008).
21. C. Maurer, A. Jesacher, S. Fürhapter, S. Bernet, and M. Ritsch-Marte, "Tailoring of arbitrary optical vector beams," New J. Phys. **9**, 78-1–20 (2007).
22. I. Freund, M.S. Soskin, and A.I. Mokhun, "Elliptic critical points in paraxial optical fields," Opt. Commun. **208**, 223–253 (2002).